Canthin-6-One 9-O-Beta-Glucopyranoside: an inhibitor of SARS-CoV-2 (COVID 19) proteases PL^{pro} and M^{pro}/ $3CL^{pro}$

Devvret Verma
Graphic Era (Deemed to be University)
Debasis Mitra
Raiganj University
Anshul Kamboj
Graphic Era (Deemed to be University)
Bhaswatimayee Mahakur
Revenshaw University
Priya Chaudhary
Banasthali University
Rakesh Shrivastav
NGF College of Engineering and Technology
Pracheta Janmeda
Banasthali University
Kumud Pant
Graphic Era (Deemed to be University)
Pradeep K. Das Mohapatra (pkdmvu@gmail.com)
Raiganj University

Research Article

Keywords: molecular docking, SARS-CoV-2 (COVID 19), medicinal plant, natural inhibitors, PLpro-Mpro/ 3CLpro

Posted Date: September 21st, 2020

DOI: https://doi.org/10.21203/rs.3.rs-81197/v1

Version of Record: A version of this preprint was published at Current Research in Pharmacology and Drug Discovery on June 5th, 2021. See the published version at https://doi.org/10.1016/j.crphar.2021.100038.

Abstract

The rapid spread of SARS-CoV-2 has raised a severe global public health issue, where therapy is not identified with specific drugs or vaccines. The present investigation dealt with the inhibition of various proteins and receptors of virus using phytocompounds of three pertinent medicinal plants *i.e. Eurycoma harmandiana*, *Sophora flavescens* and *Andrographis paniculata*. Phytocompounds known to have antiviral properties were screened against the papain-like protease (PL^{pro}) and main protease (M^{pro}) / 3-chymotrypsin-like Protease ($3CL^{pro}$). Molecular docking with Canthin-6-One 9-O-Beta-Glucopyranoside showed the highest binding affinity and least binding energy with both the proteases *viz*. PL^{pro} and M^{pro}/ $3CL^{pro}$. ADMET analysis of the compound suggested that it is having drug-like properties like high gastrointestinal (gi-) absorption, no blood-brain barrier permeability, and high lipophilicity.

Introduction

The Coronaviruses (CoVs) are composed of positive sense, large, enveloped and single-stranded copy of RNA, capable of infecting both humans and animals [1]. In December 2019, a novel kind of coronavirus resulted an upsurge of pulmonic disorder, first in the city of Wuhan, China, and there after expands around the globe. For SARS-CoV-2 infections, bats are found responsible for the origin of the virus [2]. The illness caused by SARS-CoV-2 is named as coronavirus disease 2019 (COVID-19) [3,4,5]. The CoVs are endocytosed in the lysosomes and endosome prior to the fusion with the cells. The lumen of lysosome having acidic structure (pH of 4.5) and its acidification could increase the cellular ingress of CoVs. Proton pumps involved in endocytic acid-base stability comprises of vacuolar proton-translocating ATPase (V-ATPase) which is needed for the maintenance of an acidic pH of lumen and its restriction bring the lowering of lysosomal acidification and Na/H exchanger (NHE), which regulates the pH of lumen and balance of sodium by transferring protons out in trade for cations, hence raising the pH of lumen. The NHE is regulated through the phosphorylation by the protein kinase A to endured intracellular acidosis. Therefore, acidification could be decadent by the inhibition of protein kinase A [6].

The absolute sequencing of genome revealed that the novel virus associated to a big family of coronaviruses and is intently connected to earlier SARS-CoV. During infection it codes for the two kinds of big polyproteins that are latter processed by viral proteases, main protease or 3-chymotrypsin-like protease (M^{pro}/$3CL^{pro}$) and papain-like proteases (PL^{pro}) [7,8]. M^{pro}/$3CL^{pro}$ take part in viral maturation and replication, thus can assist as the principal drug target. To know the structural modification of M^{pro}/$3CL^{pro}$, certain sequence similarity and phylogenetic network analysis were performed, that portrayed division of Coronaviridae M^{pro}/$3CL^{pro}$ in to five groups particular to viral hosts. Furthermore, it has been perceived that the conformation of binding site and backbone are well conserved in spite of disparity in some of the residues [9]. The three-dimensional structure of SARS-CoV-2 is around 96% alike to that of SARS-CoV M^{pro}/$3CL^{pro}$. Domain I and II are consist of β barrels that bear the site for substrate-binding between them and Domain III comprises of helices, is intricated in managing the M^{pro}/$3CL^{pro}$ dimerization, primarily through the interaction of salt-bridge between ARG^{4} of one protomer and GLU^{290} of another [10]. Enzyme dimerization is required for catalytic activity, because the N-finger of two protomers interrelate with GLU^{166} of the another protomer and by that assist in shaping the S1 pocket of the substrate-binding area [2,10,11]. In SARS-CoV-2, the isoleucine is restored by leucine and threonine by alanine. However, the catalytic competence of SARS-CoV-2 M^{pro}/$3CL^{pro}$ is moderately greater than SARS-CoV [12]. Further the approximated dissociation constant of dimerization is similar for the two enzymes, as evaluated by analytical ultracentrifugation. So, this crystal structure is used to dock the variable natural compounds acquired from the diversified plant species [13]. This catalytic mechanism of M^{pro}/$3CL^{pro}$ mark it as a promising target for the development of drug consequently contributing viable leads [14]. PL^{pro} is a monomer with a catalytic triad (Cys-His-Glu) flanked by transmembrane domain and domain of unknown function [15]. The enzymatic activity of PL^{pro} reveals that it is a deubiquitinating (DUB) and deISGylating enzyme. It recognizes and hydrolyse the cellular proteins ubiquitin (Ub) and the UBL protein ISG15 (interferon-induced gene 15) in the host cell protein [16]. Because of the pivotal roles and crucial function, the proteases perform in the life-cycle of virus, they are crucial target for the discovery of antiviral agent design for SARS-CoV-2 COVID19 [17, 18, 19, 20, 21].

By 10^{th} August 2020, beyond 19,687,156 sufferers were documented globally, with greater than 7,27,435 of demises, which resume to rising, majorly in the USA, Western Pacific, South-east Asia, Europe, Africa, and Eastern Mediterranean, as these are nations with a huge fragment of elderly inhabitants who have been infected with the SARS-CoV-2 [22]. The solely efficacious way to prevent the scattering of SARS-CoV-2 includes isolating the citizens by implementing a strict lockdown and providing a clinical treatment to the infected individuals with acute indications [2,22]. At present, no particular drug has been invented, and hence in view of the risk factors related with this illness, there is a critical requirement for a treatment technique to nurse this ailment in order to restrict its transference [23]. Currently, the idea of drug reuse and traditional knowledge is popularly utilized for the cure of variable disorders as it lessens the time, cost, and uncertainty of the drug generation operation by using a rapid computational perspective [11,24].

Eurycoma harmandiana Pierre is a small plant, belongs to Simaroubaceae family, allocated in the dividing line between Laos and Thailand [25]. Kanchanapoom [25] isolated the two alkaloid, 7-hydroxy-β-carboline 1-propionic acid and Canthin-6-one 9-O-beta-glucopyranoside from the root part of *E. harmandiana* which are latter used as an anti-viral agent. ul Qamar [26] carried out the docking of cantin-6-one 9-O-beta-glucopyranoside with NS1 protease in order to find out its effectiveness against dengue virus. It showed hydrogen bonds with the back-bone and side chain of SER^{80} and to THR^{87} and ASN^{130} side chains.

Sophora flavescens is a small Fabaceous plant, related to Sophora genus. The roots of *S. flavescens* are termed as Kushen. It is broadly distributed in the regions of Pacific Islands, Oceanica and the Asia, and has been greatly utilized as a conventional herbal medication for the therapy of pain, scabies, myocarditis, cancer, dysentery, fever, and viral hepatitis [27]. Lin [28] reported that the Ethyl acetate (EA) extract of *S. flavescens* resulted in the better inhibition of CYP3A activity in the human liver in a dose-dependent manner as compared to water and butanol extract. Many of the compounds were isolated from the roots of *S. flavescens* but out of them, Kushenol W and Kushenol K are utilized for carried out the study of molecular docking in case of dengue virus. ul

Qamar [26] docked the Kushenol W with NS1 protease and determined its hydrogen bonding with the back-bone and side chain of ASN^{76}, with the side chains of ASN^{130} and THR^{87} and to the back-bone of GLU^{83} and Kushenol K, results hydrogen bonding with the SER^{80} back-bone.

Andrographis paniculata (Burm. F) Nees, is an herbaceous plant, belongs to Acanthaceae family. It has conventionally been utilized in China, Sri Lanka, India, and some other southeast Asian countries. This plant is broadly acknowledged for its anti-inflammatory action against the infection of upper respiratory tract [29]. Several compounds such as 3α, 14, 15, 18-tetrahydroxy-5β, 9βH, 10α-labda-8, 12-dien-16-oic acid γ-lactone, deoxyandrographolide, neoandrographolide, 14-deoxy-11, 12-didehydroandrographolide, deoxyandrographolide19β-d-glucoside, 5,7,2',3'-tetramethoxyflavanone, 5-hydroxy-7,2',3'-trimethoxyflavone, 14-Deoxy-11-oxoandrographolide, 5-Hydroxy-7,8,2',3'-Tetramethoxyflavone,5-Hydroxy-7,8,2'-Trimethoxyflavone, Andrographine, Panicoline, Paniculide-A, Paniculide-B, Paniculide-C have been reported from *A. paniculata*. According to [30] many of the physician have manufactured several derivatives of andrographolide, which manifest remarkable remedial activities such as antiviral, antifeedant, anti-HIV, antidiabetic, antitumor, antibacterial, and anti-inflammatory. The concentration and composition of chemical constituents in plants are greatly affected by variable factors like harvesting condition, growth condition, genetic factors, types of extraction solvent, and concentration of solvents [31]. Churiyah [32] indicated that the ethanol fraction of *A. paniculata* inhibited the titre of SRC virus in a similar way as done by Lamivudine control in A549 cell line. Wintachai [33] reported that andrographolide of *A. paniculata* can be employed as a curative agent against CHIKV (Chikungunya virus. So, in our investigation is concentrated on the identification of natural composite with an exclusive objective to speed up the recognition of particular medication for the treatment of SARS-CoV-2.

Materials And Methods

Medicinal plant and their natural components

A. paniculata, E. harmandiana and *S. flavescens* are highly valuable medicinal plant reported by ul Qamar, Mussard, Rafi [26,29,31] and JayaKumar [30] and others researchers and it is mainly used as an herbal remedy for the treatments of lung, sore throat, flu & upper respiratory tract infections, inhibitors activity of NS1, NS3/NS2B and NS5 proteins of dengue virus and anti-inflammatory, anti-tumor, anti-HIV, antibacterial, antifeedant, antidiabetic, antiviral & other pharmacological activities. The molecular properties of the natural components of three pertinent medicinal plant were retrieved from the PubChem database (**Table 1**, [34]).

Table 1. Details of the compounds of three traditional medicinal plant

Compounds	Compound CID	Molecular Formula	Molecular Weight (g/mol)	SMILES
E. harmandiana				
Canthin-6-One 9-O-Beta-Glucopyranoside	637482	$C_{20}H_{20}N_2O_7$	400.382	C1=CC2=C(C=C1OC3C(C(C(C(O3)CO)O)O)O)N4C(=O)C=CC5=NC=CC2=C54
S. flavescens				
Kushenol W	42608033	$C_{21}H_{22}O_7$	386.395	CC(=CCC1=C2C(=C(C=C1O)O)C(=O)CC(O2)C3=CC(=C(C=C3O)O)OC)C
Kushenol K	44428630	$C_{26}H_{32}O_8$	472.527	CC(=C)C(CCC(C)(C)O)CC1=C2C(=C(C=C1O)OC)C(=O)C(C(O2)C3=C(C=C(C=C3)O)O)O
A. paniculata				
Andrographolide (3α, 14, 15, 18-tetrahydroxy-5β, 9βH, 10α-labda-8, 12-dien-16-oic acid γ-lactone)	5318517	$C_{20}H_{30}O_5$	350.449	CC12CCC(C(C1CCC(=C)C2CC=C3C(COC3=O)O)(C)CO)O
Deoxyandrographolide	21679042	$C_{20}H_{30}O_4$	334.4	CC1=C(C2(CCC(C(C2CC1)(C)CO)O)C)CCC3=CCOC3=O
Neoandrographolide	9848024	$C_{26}H_{40}O_8$	480.6	CC1(CCCC2(C1CCC(=C)C2CCC3=CCOC3=O)C)COC4C(C(C(C(O4)CO)O)O)O
14-Deoxy-11,12-didehydroandrographolide	5708351	$C_{20}H_{28}O_4$	332.4	CC12CCC(C(C1CCC(=C)C2C=CC3=CCOC3=O)(C)CO)O
deoxyandrographolide19β-d-glucoside	71511033	$C_{32}H_{52}O_9$	580.7	CC1C2CCC(C2=CC3(C(CC(=C3C(C1O)OC4C(C(C(C(O4)COC(C)(C)C=C)O)O)O)C(C)C)O)C)COC
5,7,2',3'-tetramethoxyflavanone	12135218	$C_{19}H_{20}O_6$	344.4	COC1=CC=CC(=C1OC)C2CC(=O)C3=C(O2)C=C(C=C3OC)OC
5-Hydroxy-7,2',3'-Trimethoxyflavone	12135219	$C_{18}H_{16}O_6$	328.3	COC1=CC=CC(=C1OC)C2=CC(=O)C3=C(C=C(C=C3O2)OC)O
14-Deoxy-11-oxoandrographolide	101593061	$C_{20}H_{28}O_5$	348.4	CC12CCC(C(C1CCC(=C)C2C(=O)CC3=CC(=O)OC3)(C)CO)O
5-Hydroxy-7,8,2',3'-Tetramethoxyflavone	5319878	$C_{19}H_{18}O_7$	358.3	COC1=CC=CC(=C1OC)C2=CC(=O)C3=C(O2)C(=C(C=C3O)OC)OC
5-Hydroxy-7,8,2'-trimethoxyflavone 5-glucoside	44258542	$C_{24}H_{26}O_{11}$	490.5	COC1=CC=CC=C1C2=CC(=O)C3=C(O2)C(=C(C=C3OC4C(C(C(C(O4)CO)O)O)O)O)OC)C
Andrographine	5318506	$C_{18}H_{16}O_6$	328.3	COC1=CC=CC=C1C2=CC(=O)C3=C(O2)C(=C(C=C3O)OC)OC
Panicoline	181763	$C_{24}H_{39}NO_7$	453.6	CCN1CC2(CCC(C34C2C(C(C31)(C5(CC(C6CC4C5C6OC)OC)O)O)OC)O)CO
Paniculide-A	11821485	$C_{15}H_{20}O_4$	264.32	CC(=CCCC1=C2C(CC3(C(C2O)O3)C)OC1=O)C
Paniculide-B	101289823	$C_{15}H_{20}O_5$	280.32	CC(=CCCC1=C2C(CC3(C(C2O)O3)CO)OC1=O)C
Paniculide-C	101289824	$C_{15}H_{18}O_5$	278.3	CC(=CCCC1=C2C(CC3(C(C2=O)O3)CO)OC1=O)C

Protein preparation

The crystal structure of papain-like protease (PL^{pro}), chymotrypsin-like protease ($3CL^{pro}$ /M^{pro}) with PDB IDs 6W9C and 6M2M respectively were retrieved from the Research Collaboratory for Structural Bioinformatics Protein Databank (RCSB PDB) [https://www.rcsb.org/,35]. All the crystal structures were prepared by removing existing ligands and water molecules by PyMOLv2.3.3, which is a comprehensive molecular visualization software that enables users to observe the 3D structures of the compounds [36].

Ligand preparation

The 3D structures of phytochemicals and drugs were retrieved from the PubChem database (www.pubchem.ncbi.nlm.nih.gov) [34]. The ligands were then further converted into the .pdbqt format using open babel tool for the molecular docking [37].

Protein-molecular docking and building complexes

Molecular docking approaches are the best techniques for forecasting the reactions between drugs and macromolecules. The blind docking process includes a quest for binding sites on the entire surface of the macromolecule. The blind molecular docking analyzes of some recognized medications were screened with SARS-CoV-2 proteases along with some bioactive natural compounds. Docking of the protein targets and ligands were carried out by using AutoDock Vina Trott [38] and the interaction of the protein ligand complex was visualized using PyMOL and BIOVIA Discovery Studio 2020 [39].

ADMET

ADMET stands for Absorption, Distribution, Metabolism, Excretion and Toxicity. The prediction of the ADMET properties plays an important role in the drug discovery and development. Properties such as absorption, distribution, metabolism, excretion and toxicity (ADMET) of compounds were determined using SWISS ADME (http://www.swissadme.ch/) and is represented in Table 2. The 2 D representation of the compounds were downloaded from the PubChem database [35].

Result And Discussion

The outbreak of novel coronavirus in Wuhan region of China has become pandemic. The origin of the virus is currently unknown, but few researchers claim that it is a type of coronavirus from bat origin, some claims that it came from fishes to humans [3,40,41,42]. There were also controversial statements that it was made in a laboratory or otherwise engineered and after research the statement got contradicted by the Scripps Research Institute and stated that the virus has natural origin [43]. The literatures have very few information about the mechanism of action and even the detailed information about the genetic material and proteins of SARS-CoV-2 is in scarce. The situation is becoming worse day by day as the therapeutics for the COVID-19 is not available yet. The drug repurposing strategy is being used to somehow cure of the patients. Recently few drugs have been sent for clinical trials and few of them have even passed second stage. The drug and vaccine discovery process is still on and no lead has come in market as an armamentarium against the disease [16,44] till date. Therefore, there is a need of therapeutics still persist. The compounds derived from plants have gain much more acknowledgement in recent time and hence can be used as possible solution against the disease. Molecular docking is the finest way to predict the binding affinities of compounds and hence, plays a pivotal role in discovery and development of drugs [45].

The novel corona virus has viral genome which encodes for the 20 proteins, which includes two protease PL^{pro} and $3CL^{pro}/M^{pro}$) that plays a crucial role in viral replication and gained tremendous attention as a drug target. In the current study, these two proteases have been taken as a potential target [46]. Eighteen phytocompounds from the three medicinal plants viz. *E. harmandiana*, *S. flavescens* and *A. paniculate* were considered for the molecular docking analysis (Table 1). Chloroquine, Oseltamivir, Remdesivir and Ribavirin has been used as a control. These drugs have been recently used in the treatment of the COVID-19 patients and are in clinical trial. There is no potential drug molecule approved by the FDA and this is the only reason that these repurposed drugs have been taken as a control in the current study. Chloroquine is an antimalarial drug is being used in combination with Azithromycin for the treatment of COVID patients [47]. Oseltamivir in combination with hydroxychloroquine was also found to inhibit the coronavirus to some extent [48,49]. Remdesivir and ribavirin are the FDA-approved anti-RdRp drugs that was found to treat patients and reduce the danger of the mysterious new viral infection COVID-19 [50]. Binding energies of various natural occurring phytochemicals were obtained through AutoDock Vina. The interaction of inhibitor and protein receptor were predicted in 2D and 3D, with the help of BIOVIA Discovery study visualizer. The docked poses clearly show that drug molecules and phytocompounds bind the active sites of SARS-COV-2 macromolecule structures.

Interaction with PL^{pro}

Panicoline binds firmly with the residue GLY^{160} through conventional hydrogen bond, GLN^{269} GLY^{160} through carbon-hydrogen and Van der Waals with the surrounding residues of the PL^{pro} protein of SARS-COV-2 (**Figure 1a**). 14-Deoxy-11,12-didehydroandrographolide stabilizes the active site through conventional hydrogen bond (GLN^{269}), carbon hydrogen bond (GLY^{160}) and Van der Waals interaction with rest residues (**Figure 1b**). Canthin-6-One 9-O-Beta-Glucopyranoside append within the active site of SARS-COV-2 through Pi-anion interaction with residues GLU^{161}, conventional hydrogen bond with residue LEU^{162}, GLY^{160}, ASN^{109}, Pi donor hydrogen bond with LEU^{162} and Van der Waals interaction with the rest (**Figure 1c**). Andrographine secured the active sites with amide-pi stacked interaction with residues GLY^{161}, conventional hydrogen bond with ASN^{109}, carbon hydrogen bond with ASP^{108}, pi-alky, alkyl interaction with the residues LEU^{162}, HIS^{89}, VAL^{159} and Van der Waals interaction with the surrounding residues (**Figure 1d**). Andrographolide adhere within the active sites through conventional hydrogen bond (VAL^{159} and GLN^{269}) and with the Van der Walls interaction with the rest residues as shown in **Figure 1(e**). 5-Hydroxy-7,8,2',3'-Tetramethoxyflavone firmly stabilizes the active sites through amide pi-stacked interaction with residues GLY^{160}, conventional hydrogen bond with ASN^{109}, carbon hydrogen bond with ASP108, GLN269, further it undergoes alkyl, pi-alkyl interaction with residues LEU^{162}, VAL^{159}, HIS^{89} and through Van der Waals interaction with the rest (**Figure 1f**). Neoandrographolide binds with the active sites through conventional hydrogen bond (ASN^{109}, GLN^{269}, VAL^{159}) and through carbon hydrogen bond (GLY^{160}, THR^{158}) (**Figure 1g**). Paniculide-A stabilizes the active site of the PL pro through alkyl interaction with residues VAL^{159} and conventional hydrogen bond with residues ASN^{109} (**Figure 1h**). The 5-Hydroxy-7,2',3'-Trimethoxyflavone cohere with the active sites with residues LEU^{162}, VAL^{159}, HIS^{89} through alkyl, pi-alkyl interaction, pi-anion interaction with residue GLY^{160}, conventional hydrogen bond with residues THR^{158}, ASN^{109} and carbon hydrogen bond with residues ASN^{109} and with rest through Van der Walls interaction as shown in **Figure 1(i).** 5,7,2',3'-tetramethoxyflavanone forms several noncovalent interaction at the active site, it forms conventional hydrogen bond with THR^{158}, ASN^{109}, carbon hydrogen bond with residue GLN^{269}, alkyl and pi-alkyl bond with LEU^{162}, HIS^{89}, VAL^{159} and pi-anion interaction with residue GLU^{161} (**Figure 1j**). Deoxyandrographolide stabilizes the active

site only through single conventional hydrogen bond (GLN269) and surrounding residues with Van der Waals interaction (**Figure 1k**). Kushenol W form pi-sigma interactions with GLU^{161}, pi alkyl bond with LEU^{162}, conventional hydrogen bond with GLY^{160} carbon hydrogen bond with residues ASP^{108} and GLY^{160} (**Figure 1l**). The Kushenol K forms conventional hydrogen bonds with LEU^{162}, ASN^{109}, carbon-hydrogen bond with VAL^{159} and Van der Waals interaction with the surrounding residues (**Figure 1m**). 5-Hydroxy-7,8,2'-trimethoxyflavone 5-glucoside secure the active site through amide pi stacked interactions with residues GLY^{160}, pi-anion interaction with GLU^{161} and conventional hydrogen bond with GLN^{269}, ASN^{109} (**Figure 1n**).

Deoxyandrographolide19β-D-glucoside cohere active sites through conventional hydrogen bond with residue THR^{158}, carbon hydrogen bond with residues GLY^{160}, ASP^{108} and alkyl bond with residue LEU^{162} and it is depicted in form of 2D representation in **Figure 1(o)**. Paniculide-B forms alkyl bond with VAL^{159}, conventional hydrogen bond with ASN^{109}, GLY^{160}, GLN^{269}, and carbon hydrogen bond with GLN^{269} and where Paniculide-C secure the active sites with alkyl (LEU^{162}), conventional hydrogen bond (ASN^{109}) (**Figure 1p** and **1q)**. The interaction analysis of 14-Deoxy-11-oxoandrographolide depicts that it cohere the active sites through conventional bond with residues LEU^{162}, ASN^{109} and GLN^{269} (**Figure 1r**).

Van der Wall interactions and hydrogen bonding play a major role in the binding process. Van der Wall interaction is a weakest intermolecular attraction between two molecules. Though it is the weakest bond between two objects, but a lot of Van der Wall forces can make the interaction very strong [51]. In the protein ligand interactions, the hydrogen bond helps the ligand to stabilize but there are also other interactions such as hydrophobic or Van der Wall interactions that helps in stabilization of the nonpolar ligands too. An analysis of the structure of ligands and docked poses usually helps in understanding the interactions and the binding energy establishes which of the compound is important. Based on these basics the molecular docking program is most widely used tool in the drug discovery process as the result suggests the potential drug compound based on least binding energy [52]. The comparison of the estimated free energy of binding (ΔG) or binding affinity inferred that the Canthin-6-One 9-O-Beta-Glucopyranoside (-9.4 kcal/mol) have the least binding energy among the studied plant natural components and can be a potential drug against the PLpro of SARS COV-2. The order of binding energy of other studied plant natural components is as follows: 5-Hydroxy-7,8,2'-trimethoxyflavone 5-glucoside (-8.8 kcal/mol) > 14-Deoxy-11-oxoandrographolide (-8.7 kcal/mol) > Kushenol K and Neoandrographolide (-8.6 kcal/mol) > Kushenol W (-8.4 kcal/mol) > 14-Deoxy-11,12-didehydroandrographolide (-8.2 kcal/mol) > Deoxyandrographolide (-8.1 kcal/mol) > Paniculine (-8.0 kcal/mol) > Andrographolide and Deoxyandrographolide19β-D-glucoside (-7.9 kcal/mol) > 5-Hydroxy-7,8,2',3'-Tetramethoxyflavone and Andrographine (-7.6 kcal/mol) > 5,7,2',3'-tetramethoxyflavanone and 5-Hydroxy-7,2',3'-Trimethoxyflavone (-7.5 kcal/mol) > Paniculide-B (-7.2 kcal/mol) > Paniculide-A (-7.1 kcal/mol) > Paniculide-C (-6.7 kcal/mol). The analysis of binding energies suggests that all the binding energy falls between -6.7 to 9.4 kcal/mol and 2D interaction in **Figure 1(a-r)** depicts that the studied phytocompounds have a lot of hydrogen bond and Van der Walls interaction that suggests that the ligands are stabilized within the complex.

Interaction with M^{pro}/$3CL^{pro}$

The Panicoline secures active sites of the main protease (M^{pro} or $3CL^{pro}$) through conventional hydrogen bond and carbon hydrogen bond with residues ASN^{151}, THR^{111}, GLN^{110}, SER^{158} and ILE^{152} respectively (**Figure 2a**). 14-Deoxy-11,12-didehydroandrographolide forms conventional hydrogen bond with residues THR^{111} and pi-alkyl interaction with ILE^{249} and van der Waals interaction with the surrounding residues (**Figure 2b**). Canthin-6-One 9-O-Beta-Glucopyranoside binds firmly with the active sites through conventional hydrogen bond with residues THR^{111}, ASP^{295}, THR^{292} and pi-alkyl bond with VAL^{202} (**Figure 2c**). Andrographine adhere within the active sites through conventional hydrogen bond with the residue THR^{292}, pi-pi stacked interaction with the residue PHE^{294} and pi-alkyl bond with PRO^{293}, ILE^{294} (**Figure 2d**). Andrographolide forms conventional hydrogen bond with residue ASN^{151}, pi-sigma bond with residue PHE^{294} and van der Waals interaction with the surrounding residues (**Figure 2e**). Neoandrographolide forms conventional hydrogen bond with the residues ASP^{295}, THR^{111} and pi alkyl interaction with residues VAL^{202}, PRO^{293} and ILE^{249} (**Figure 2f**). Paniculide-A cohere the active sites of the main protease (M^{PRO} or $3CL^{PRO}$) with conventional hydrogen bond and alkyl,pi-alkyl interaction with the residues GLN^{110}, THR^{111}, THR^{292} and ILE^{249}, PHE^{294}, PHE^{8} respectively (**Figure 2g**). 5-Hydroxy-7,8,2',3'-Tetramethoxyflavone adhere with the active sites through conventional hydrogen bond (ASN^{151} and THR^{111}), pi donor hydrogen bond (THR^{292}), pi-pi-stacked (PHE^{294}), pi- alkyl interaction with residues PRO^{293}, ILE^{294}, PHE^{294} and are depicted in **Figure 2(h)**. 5,7,2',3'-tetramethoxyflavanone forms Pi alkyl interaction, conventional hydrogen bond pi-pi stacked interaction with residues ILE^{249}, THR^{111} and PHE^{294} respectively (**Figure 2i**). 5-Hydroxy-7,2',3'-Trimethoxyflavone stabilizes the active sites through conventional hydrogen bond (ASN^{151} and THE^{111}), pi donor hydrogen bond (THR^{292}), pi-pi stacked interaction (PHE^{294}), alkyl, pi-alkyl interaction (PHE^{294}, ILE^{249}, HIS^{246} and PRO^{293}) and Van der Waals interaction with the surrounding residues and the interactions can be seen in Figure **2(j)**. With a good efficiency of binding Deoxyandrographolide forms conventional hydrogen bond with ASN^{151} and pi-alkyl with PHE^{249} (**Figure 2k**). Kushenol W cohere with active sites residues THR^{111} through conventional hydrogen bond, pi-pi stacked interaction (PHE^{294}) and pi alkyl interactions (ILE^{249} and PRO^{293}) (**Figure 2l**). 5-Hydroxy-7,8,2'-trimethoxyflavone 5-glucoside forms conventional hydrogen bond with residue GLN^{110}, Pi-sigma interaction (PHE^{294}), pi-pi interaction with PHE^{294}, alkyl, pi-alkyl interaction with VAL^{297}, PRO^{293}, ILE^{249} and carbon hydrogen bond with ILE^{249} (**Figure 2m**). Kushenol K stabilizes the active site with residues PHE^{294} through pi-pi stacked interaction, pi-pi sigma interaction (ILE^{249}) and pi-alkyl interacions (PRO^{293} and PHE^{294}) (**Figure 2n**). The Deoxyandrographolide19β-d-glucoside forms conventional hydrogen bond with residue THR^{21}, THR^{26}, GLN^{69}, ILE^{249} and carbon hydrogen bond with ASP^{245} (**Figure 2o**). Paniculide-B cohere with the active sites through conventional hydrogen bond (THR^{292}, THR^{111} and GLN^{110}) and alkyl interaction (PHE^{8} and PHE^{294}) whereas Paniculide-C forms conventional hydrogen bond with THR^{111} and GLN^{110}; alkyl and pi alkyl interaction with PRO^{293}, HIS^{246}, ILE^{249}, VAL^{202} and the interactions are depicted in **Figure 2(p and q)**. In the case of 14-Deoxy-11-oxoandrographolide, it stabilizes the active sites with residue GLN^{269}, ASN^{109} and LEU^{162} through conventional hydrogen bond, alkyl bond with ILE^{249} and through Van der Waals interaction with the rest residues (**Figure 2r**).

The least binding energy of Canthin-6-One 9-O-Beta-Glucopyranoside (-8.5 kcal/mol) obtained from molecular docking study suggests that the molecule have good binding affinity against the M^{pro} or $3CL^{pro}$. The order of other molecules as per free energy binding (ΔG) is as follows: Neoandrographolide (-8.4 kcal/mol) > Kushenol W (-7.3 kcal/mol) > 14-Deoxy-11,12-didehydroandrographolide and 14-Deoxy-11-oxoandrographolide (-7.1 kcal/mol) > 5-Hydroxy-7,8,2'-

trimethoxyflavone 5-glucoside & Andrographolide (-6.9 kcal/mol) > 5-Hydroxy-7,2',3'-Trimethoxyflavone (-6.8 kcal/mol)> 5,7,2',3'-tetramethoxyflavanone, 5-Hydroxy-7,8,2',3'-Tetramethoxyflavone, Andrographine and Paniculine (-6.5 kcal/mol) > Kushenol K (-6.4 kcal/mol) > deoxyandrographolide19β-d-glucoside or diterpene glucoside (-6.2 kcal/mol) > Paniculide-A (-6.1 kcal/mol) > Paniculide-C (-6.0 kcal/mol) Paniculide-B (-5.9 kcal/mol). The 2D and 3D interaction is depicted in the **Figure 2 (a-r)**.

Interaction with control drugs

The docked pose of minimum energies conformers of four control drugs Chloroquine, Oseltamivir, Remdesivir and Ribavirin. **Figure 3 (a-d)** shows chloroquine binds firmly with PL^{PRO} active site and form conventional hydrogen bond with THR^{158} residue and carbon hydrogen bond with residue GLU^{161} and VAL^{159}. Oseltamivir stabilizes within active site through conventional bond with residue ASN^{109}, carbon hydrogen bond with residue GLY^{160} and alkyl interaction with residue LEU^{162}. Remdesivir binds to the active site through pi-anion (GLU^{161}), amide-pi stacked interaction (VAL^{159} and GLY^{160}), conventional hydrogen bond (ASN^{109}) and pi-alkyl interaction (LEU^{162}). Ribavirin forms conventional hydrogen bond with residue GLY^{160}, GLN^{269}, LEU^{162}, ASN^{109}, carbon hydrogen bond with residue GLN^{269}, ASN^{109} and among all the interactions Van der Walls interaction plays a major role. The comparison of binding affinity or estimated free energy (ΔG value) of binding shows that the Remedisivir (-8.4 kcal/mol) have least binding energy with active sites of the PL^{pro}. The order of binding energy of other drugs with PL^{pro} is as follows: Ribavirin (-6.8 kcal/mol) > Oseltamivir (-6.4 kcal/mol) > Chloroquine (-6.3 kcal/mol).

Interactions of the drugs with the $M^{pro}/3CL^{pro}$ shows that chloroquine firmly binds within the active sites through pi-anion interaction with the residues ASP^{295}, pi-pi stacked interaction with residues PHE^{294} and pi-alkyl interaction with residue PHE^{294} and carbon hydrogen bond with residue THR^{111}. It doesn't form any hydrogen bonds within the active site. Ribavirin forms conventional hydrogen bond with residues GLN^{110}, PHE^{294}, THR^{111}, THR^{292}. Oseltamivir stabilises the pi- alkyl interaction with PHE^{294} and conventional hydrogen bond with residues GLN^{110}, THR^{111} and ASN^{151}. Remdesivir cohere the active site through conventional hydrogen bond (GLN^{110}, ASN^{151} and PHE^{294}) and pi-alkyl interaction (ILE^{249}, PRO^{252}, VAL^{297} and PRO^{293}) with the active sites of $M^{pro}/3CL^{pro}$. Pi – interaction plays a major role in stability of a particular drug within the active site [68]. The binding affinity of the drugs with $M^{pro}/3CL^{pro}$ suggests that the Remdesivir have high affinity to inhibit the protein with most negative ΔG value i.e. - 8.3 kcal/mol and all the other studied drugs showed similar ΔG value i.e. -5.8 kcal/mol, the 3D and 2D interactions of drugs with the active sites of $M^{pro}/3CL^{pro}$ are depicted in Figure **4 (a-d)**.

Pharmacokinetics

ADMET stands for Absorption, Distribution, Metabolism, Excretion and Toxicity. The prediction of the ADMET properties plays an important role in the drug discovery and development. The absorption of drugs depends on membrane permeability, intestinal absorption, skin permeability levels, P-glycoprotein substrate or inhibitor. The distribution of drugs depends on factors that include the blood–brain barrier (logBB), CNS permeability, and the volume of distribution (VDss). Metabolism is predicted based on the CYP models for substrate or inhibition (CYP2D6, CYP3A4, CYP1A2, CYP2C19, CYP2C9, CYP2D6, and CYP3A4). Excretion is predicted which is based on the total clearance model and renal OCT2 substrate. The toxicity of drugs is predicted based which is on AMES toxicity, hERG inhibition, hepatotoxicity, and skin sensitization. These parameters were calculated and checked for compliance with their standard ranges [54]. Properties such as ADMET profiling of compounds were determined using SWISS ADME [http://www.swissadme.ch/, 53]. Intestinal epithelium barrier/gut–blood barrier is a barrier that is crucial barrier for all the compounds to overcome. Intestinal epithelium barrier regulates nutrients absorption, water and ion fluxes, and denotes the first defensive barrier against toxins and enteric pathogens and the gut-blood barrier (GBB) controls the passage of drugs from intestinal lumen to the bloodstream. Except Kushenol K, GI absorption of all the phytochemicals were high which means that it was predicted to be absorbed easily in gut and intestine epithelium. Distribution of compounds through various compartments of the body was accessed using its Blood-brain barrier (BBB) penetration [55]. Among all the phytocompounds only Panculide-A, Andrographine, Deoxyandrographolide, 5,7,2',3'-tetramethoxyflavanone, 5-Hydroxy-7,2',3'-Trimethoxyflavone are predicted to have blood brain barriers penetration. P glycoprotein is a drug transporter having broad substrate specificity, Drugs that are substrates of P-gp are subject to low intestinal absorption, low blood-brain barrier permeability, and face the risk of increased metabolism in intestinal cells. 14-Deoxy-11,12-didehydroandrographolide, 5-Hydroxy-7,8,2'-trimethoxyflavone 5-glucoside, Andrographolide, Paniculine A, Neoandrographolide, Kushenol K, 14-Deoxy-11-oxoandrographolide, Deoxyandrographolide are predicted to have affinity for p-glycoprotein. The result shows that except these phytochemicals rest phytochemicals may act as a non-substrate of p-glycoprotein [56]. Metabolism mainly depends on the CYP450 enzyme and its iso forms which are CYP 3A4, 2D6, 1A2, 2C9 and 2C19. These enzymes are responsible for the detoxification of drugs passing the liver. Therefore, any compound blocking P450 can cause toxicity. Out of all the 18 compounds 5-Hydroxy-7,8,2'-trimethoxyflavone 5-glucoside, Neoandrographolide, Kushenol W, Kushenol K, Andrographine, 5-Hydroxy-7,8,2',3'-Tetramethoxyflavone, 14-Deoxy-11,12-didehydroandrographolide, 5,7,2',3'-tetramethoxyflavanone, 5-Hydroxy-7,2',3'-Trimethoxyflavone compounds block the enzyme responsible for detoxification and hence, can be responsible for toxicity. Skin permeation coefficient (log Kp) is the measure of skin to absorb a certain drug or chemical. In the given table 2, log kp of skin permeation of all the compounds lies between the standard value of log Kp -8.0 to -1.0 cm/s except 5-Hydroxy-7,8,2'-trimethoxyflavone 5-glucoside, Deoxyandrographolide19β-D-glucoside, Paniculine, which shows that these possess an ability to absorb less in the membrane [57].

ADMET study of all these molecules suggested that the molecules Canthin-6-One 9-O-Beta-Glucopyranoside, deoxyandrographolide 19β-d-glucoside or diterpene glucoside, Paniculide-B, Paniculide-C have passed all the barriers of ADMET and indicated that these molecule can be a successful drug molecule. All these compounds have high gastrointestinal absorption which is an important and decision making standard of oral dosing, this implies that the phytocompounds can be used as an oral drug. These drugs also passed the blood brain barrier (BBB) permeability test, therefore, these compounds qualifies a fundamental index of drug distribution. High negative value of log Kp suggests that the phytocompounds have less skin permeation. Binding of CYP450 enzyme may cause degradation of phytocompounds inside the body and can lead to toxicity. Bioavailability of these compounds are high and it indicates high potential as drug molecule. The above mentioned parameters for all these molecules are in the range found for successful drug molecule (**Table 2**).

Potential drug against COVID 19

The molecular docking studies have been carried out using 19 phytocompounds that might act as potential drug against SARS-CoV-2 M^{pro}/$3CL^{pro}$ and PL^{pro}. The analysis of molecular interaction between the active sites of the studied protein and the phytocompounds suggested that these compounds can inhibit the protein and will block the viral replication. The active site of M^{pro}/$3CL^{pro}$ consists of residues THR^{21}, THR^{26}, GLN^{69}, GLN^{110}, THR^{111}, ASN^{151}, HIS^{246}, ILE^{249}, THR^{292} and ASP^{295} whereas the active site residues for PL^{pro} are ASN^{109}, THR^{158}, VAL^{159}, GLY^{160}, LEU^{162} and GLN^{269} (**Table 3**). The Canthin-6-One 9-O-Beta-Glucopyranoside in comparison with the control drugs, was found showing least binding energy with active sites of both the target proteins i.e. M^{pro}/$3CL^{pro}$ and PL^{pro}. The distance between the ligand and catalytic residues of the protein shows that the Canthin-6-One 9-O-Beta-Glucopyranoside interact within the active site of the protease proteins and have high affinity of binding. The ADMET study also suggest that the Canthin-6-One 9-O-Beta-Glucopyranoside have all the drug like properties and can be considered as a potential drug against the infection caused by human SARS coronavirus-2.

Table 3. Tabular representation of conventional hydrogen bonding and its length in protein ligand interactions

Name	SARS COV Protein 1(3CL^{pro})		SARS COV Protein 2 (PL^{pro})	
	Vital residues for H-bond formation	Length (in Å)	Vital residues for H-bond formation	Length (in Å)
Panicoline	ASN^{151} THR^{111} GLN^{110}	1.99 3.00 3.12	GLY^{160}	1.87
14-Deoxy-11,12-didehydroandrographolide	THR^{111}	3.08, 2.94	GLN^{269}	2.72
Canthin-6-One 9-O-Beta-Glucopyranoside	THR^{111} THR^{292} ASP^{295}	2.00, 2.67 2.77 2.23	LEU^{162} GLY^{160} ASN^{109}	3.05 2.16 2.99
Andrographine	THR^{111} ASN^{151}	3.20, 2.97 2.14	ASN^{109}	3.02
Andrographolide	ASN^{151}	2.46	VAL^{159} GLN^{269}	2.63 1.99, 2.51
Neoandrographolide	THR^{111} ASP^{295}	3.13, 2.71, 2.31 2.46	GLN^{269} ASN^{109} VAL^{159}	2.84, 2.08 2.68, 2.88, 3.08 3.17
Paniculide-A	GLN^{110} THR^{111} THR^{292}	3.28 2.89, 3.27 2.94	ASN^{109}	3.00, 3.06
5-Hydroxy-7,8,2',3'-Tetramethoxyflavone	THR^{111} ASN^{151}	2.99, 3.14 2.11	ASN^{109}	3.31
5,7,2',3'-tetramethoxyflavanone	THR^{111}	3.29, 3.12	THR^{158} ASN^{109}	3.13 3.13
5-Hydroxy-7,2',3'-Trimethoxyflavone	ASN^{111} ASN^{151}	3.07, 3.17 2.60	THR^{158} ASN^{109}	3.02 3.11
Deoxyandrographolide	ASN^{151}	3.02	GLN^{269}	3.12
Kushenol W	THR^{111}	3.08	GLY^{160}	1.79
5-Hydroxy-7,8,2'-trimethoxyflavone 5-glucoside	GLN^{110}	3.27	ASN^{109}	3.31
Kushenol K	NO INTERACTION		LEU^{162} ASN^{109}	3.14, 3.23 2.58
Deoxyandrographolide19β-d-glucoside	THR^{21} GLN^{69} THR^{26} ILE^{249}	2.74 3.08, 3.00 2.59, 2.49 2.70	THR^{158}	2.99
Paniculide-B	GLN^{110} THR^{292} THR^{111}	3.29 2.94 2.89, 3.33	ASN^{109} GLY^{160} GLN^{269}	3.20, 3.11, 2.80 2.73 3.37

Paniculide-C	THR^{111}	3.33, 3.19	ASN^{109}	3.05, 3.25
	GLN^{110}	2.81		
14-Deoxy-11-oxoandrographolide	GLN^{110}	3.10	LEU^{162}	2.89
	HIS^{246}	2.82	GLN^{269}	1.98
	THR^{111}	2.76	ASN^{109}	3.05

Das [58] studied 33 molecules through the help of docking approach, and find out that these molecules could bind near the Cys^{145} and His^{41} (catalytic residue) of the main protease. Salim [59] reported that α- hederin and Nigellidine are the major phytochemical obtained from *Nigella sativa* which are capable in restricting SARS-CoV-2 with great energy score as compared to clinical drugs on the basis of molecular docking. Muralidharan [11] performed molecular dynamics (MD) simulations in order to evaluate the interconnection among the protein and three drugs. The RMSD (root-mean-square-deviation) of interconnection is found to be 3Å and remain firm while the simulations. Therefore, the amalgam of ritonavir, lopinavir, and oseltamivir are greatly efficacious against the protease of SARS-CoV-2, and these agents can be surveyed further for drug reusing purpose for the victorious restriction of SARS-CoV-2. Joshi [9] identified some natural compounds such as phyllaemblicin B, hesperidin, biorobin, afzelin, nympholide A, lacticopicrin 15-oxalate, myricitrin, nympholide A, and d-viniferin from the screening of ~7100 molecules which proved as a strong binders not only for proteases but also for other targets (RNA dependent RNA polymerase, and human angiotensin-converting enzyme of SARS-CoV-2. Adeoye [6] determined the inhibitory potentiality of chloroquine, lopinavir, remdesivir, ribavirin, azithromycin, and oseltamir towards viral proteases, V-ATPase, SARS-CoV spike glycoprotein/ACE-2 complex, and protein kinase A. It was evaluated that, lopinavir has the greatest affinities for the 3-chymotrypsin like protease, cyclic AMP-dependent protein kinase A, and SARS-CoV spike glycoprotein/ACE-2 complex whereas remdesivir has shown affinities for papain-like proteins, and vacuolar proton-translocating (V-ATPase), and chloroquine has affinities for cyclic AMP-dependent protein kinase A, and 3-chymotrypsin-like protease in comparison to ribavirin and oseltamivir [60]. Aanouz [61] used the docking process for examining the interaction type and affinity at the binding site among the 67 compounds and the SARS-CoV-2 proteases. The results showed that, only three molecules (b-Eudesmol, Crocin, and Digitoxigenin) are found as inhibitors in the control of SARS-CoV-2). Enmozhi [69] evaluated out andrographolide from *A. paniculata* as a main protease inhibitor in case of SARS-CoV-2 through *in silico* studies. Kumar [62,63] carried out molecular docking study of FDA approved drugs that are used in the cure of different viral ailments in order to investigate their binding affinity for the active site of M^{pro} [64]. Docking studies determined that drugs raltegravir, tipranavir, and lopinavir-ritonavir among others particularly binds to the protease with similar affinity as of the α-ketoamide inhibitors [11]. From the earlier time, herbal plants products are successfully employed for the cure of several viral disorders. Many of the promising lead natural compounds of our investigation are anti-virals, therefore, there is a big probability that these bioactive constituents would be appropriate in the control of SARS-CoV-2 and could be helpful for the discovery of multi-targeted agent against the SARS-CoV-2 COVID19 infection [65].

The hunt for plant-derived antiviral for the control of SARS-CoV-2 is hopeful, as many plants have been reported to be effective against Beta coronaviruses [66,67]. Many reports to recognize the promising inhibitors of SARS-CoV-2 from plants have been published by using a computational approach (Das, 2020). In the present study, after evaluating the multiple medicinal properties of the natural products, a total 18 compounds (Canthin-6-one 9-O-beta-glucopyranoside from *E. harmandian;* Kushenol W, and Kushenol K from *S. flavescens*; and 3*α*, 14, 15, 18-tetrahydroxy-5*β*, 9*β*H, 10*α*-labda-8, 12-dien-16-oic acid *γ*-lactone, deoxyandrographolide, neoandrographolide, 14-deoxy-11, 12-didehydroandrographolide, deoxyandrographolide19β-d-glucoside, 5,7,2',3'-tetramethoxyflavanone, 5-hydroxy-7,2',3'-trimethoxyflavone, 14-Deoxy-11-oxoandrographolide, 5-Hydroxy-7,8,2',3'-Tetramethoxyflavone, 5-Hydroxy-7,8,2', Trimethoxyflavone, Andrographine, Panicoline, Paniculide-A, Paniculide-B, Paniculide-C from *A. paniculate*) were screened out for determining their inhibitory potentiality against M^{pro} and PL^{pro} by molecular docking analysis.

Conclusion

The current study is screening based study performed with the assistance of molecular docking and ADMET analysis tools/server and is now subject of matter to examine the activity of the compound potency of Canthin-6-One 9-O-Beta-Glucopyranoside in inhibiting SARS-CoV-2 M^{pro}/3CL^{pro} and PL^{pro}.

Summary points

- The continuing SARS-CoV-2 pandemic makes us worryingly noticed that our present choices for nursing against deadly coronavirus disease are very restricted. Therefore, there is an instant need for the discovery of novel inhibitors attacking the vital viral proteins.
- The compounds of the three plants *viz. harmandiana, S. flavescens* and *A. paniculata* were screened for antiviral activity against the proteases of the 2019-nCov or SARS COV-2.
- The molecular docking and ADMET analysis suggest that with least binding energy and drug-likeness properties Canthin-6-One 9-O-Beta-Glucopyranoside is a potential molecule that binds to the M^{pro}/3CL^{pro} and PL^{pro} and can inhibit the activity of replication and transcription of the virus and finally stop the multiplication of the virus.

Declarations

Conflict of Interest

The authors declare that there is no conflict of interest.

Author Contributions

DM, DV and BM contributed equally as first authors. DM, DV, BM, PC, AK was involved in the writing; DV, DM, KP, RS, PKDM, JP was involved in manuscript refinement & important intellectual content discussion; DV, AK was involved in molecular docking and BM, DM, DV initiated the idea of the study.

Acknowledgments

The authors are thankful to Graphic Era (Deemed to be University), Dehradun, Uttarakhand and Raiganj University, Raiganj - 733 134 Uttar Dinajpur, West Bengal India for the encouragement and support needed in the present investigation. The author D. Mitra is grateful to Government of West Bengal, India for Swami Vivekananda Merit Cum Means Ph.D. Scholarship (WBP191584588825). The authors thank the reviewers for their valuable suggestions to increase the scientific quality of the manuscript.

References

1. Jo S, Kim S, Shin DH, & Kim MS. Inhibition of SARS-CoV 3CL protease by flavonoids. *Enzyme Inhib. Med. Chem*. 35(2019).
2. Mori M, Capasso C, Carta F, Donald AW, & Supuran CT. A deadly spillover: SARS-CoV-2 outbreak. *Expert Opin. Ther. Pat*. doi: 10.1080/13543776.2020.1760838 (2020).
3. Zhang L, Shen FM, Chen F, & Lin Z. Origin and evolution of the 2019 novel coronavirus. *Infect. Dis*. doi: 10.1093/cid/ciaa112 (2020a).
4. Mohamed AH, & Fatima AJ. Covid-19 induced superimposed bacterial infection. *Biomol. Struct. Dyn*., 1-18. doi: 10.1080/07391102.2020.1772110 (2020).
5. Chaudhary P, & Janmeda P. Spreadable virus of the 21st century: COVID-19. *Conserv. J*. 21(1&2), 13-18. https://doi.org/10.36953/ECJ.2020.211202 (2020).
6. Adeoye AO, Oso BJ, Olaoye IF, Tijjani H, & Adebayo AI. Repurposing of chloroquine and some clinically approved antiviral drugs as effective therapeutics to prevent cellular entry and replication of coronavirus. *J Biomol Struct Dyn*. https://doi.org/10.1080/07391102.2020.1765876 (2020).
7. de Oliveira OV, Rocha GB, Paluch AS, & Costa LT. Repurposing approved drugs as inhibitors of SARS-CoV-2 S-protein from molecular modeling and virtual screening. *Biomol. Struct. Dyn*., 1-14 (2020).
8. Khan RJ, Jha RK, Amera GM, Jain M, Singh E, Pathak A, Singh RP, Muthukumaran J, & Singh AK. Targeting SARS-CoV-2: a systematic drug repurposing approach to identify promising inhibitors against 3C-like proteinase and 2'-O-ribose methyltransferase. *Biomol. Struct. Dyn*., 1-14 (2020a).
9. Joshi RS, Jagdale SS, Bansode SB, Shankar SS, Tellis MB, Pandya VK, Chugh A, Giri AP, & Kulkarni MJ. Discovery of potential multi-targeted-directed ligands by targeting host-specific SARS-CoV-2 structurally conserved main protease. *Biomol. Struct. Dyn*. doi: 10.1080/07391102.2020.1760137 (2020).
10. Chang GG. Quaternary Structure of the SARS Coronavirus Main Protease. In: Lal S. (eds) Molecular Biology of the SARS-Coronavirus. Springer, Berlin, Heidelberg, (2010).
11. Muralidharan N, Sakthivel R, Velmurugan D, & Gromiha MM. Computational studies of drug repurposing and synergism of lopinavir, oseltamivir and ritonavir binding with SARS-CoV-2 Protease against COVID-19. *Biomol. Struct. Dyn*.,1-6 (2020).
12. Luo Z, Matthews AM, & Weiss SR. Amino acid substitutions within the leucine zipper domain of the murine coronavirus spike protein cause defects in oligomerization and the ability to induce cell-to-cell fusion. *J Virol*. 73, 8152-8159 (1999).
13. Zhang L, Lin D, Sun X, Curth U, Drosten C, Sauerhering L, Becker S, & Rox K, Hilgenfeld R. Crystal structure of SARS-CoV-2 main protease provides the basis for design of improved α-ketoamide inhibitors. *Science* 368, 409-412. doi: 10.1126/science.abb3405 (2020b).
14. Gyebi GA, Ogunro OB, Adegunloye AP, Ogunyemi OM, & Afolabi SO. Potential inhibitors of coronavirus 3-chymotrypsin-like protease (3CLpro): an *in silico* screening of alkaloids and terpenoids from African medicinal plants. *Biomol. Struct. Dyn*. doi: 10.1080/07391102.2020.1764868 (2020).
15. Khan SA, Zia K, Ashraf S, Uddin R, & Ul-Haq Z. Identification of chymotrypsin-like protease inhibitors of SARS-CoV-2 via integrated computational approach. *Biomol. Struct. Dyn*., 1-10 (2020b).
16. Báez-Santos YM, John SES, & Mesecar AD. The SARS-coronavirus papain-like protease: structure, function and inhibition by designed antiviral compounds. *Antivir Res* 115, 21-38 (2015).
17. Andrianov AM, Kornoushenko YV, Karpenko AD, Bosko IP, & Tuzikov A, Computational discovery of small drug-like compounds as potential inhibitors of SARS-CoV-2 main protease. *J Biomol Struct Dyn*. https://doi.org/10.1080/07391102.2020.1792989 (2020).
18. Ibrahim MA, Abdeljawaad KA, Abdelrahman AH, & Hegazy MEF. Natural-like products as potential SARS-CoV-2 Mpro inhibitors: *in-silico* drug discovery. *Biomol. Struct. Dyn*., 1-13 (2020).
19. Arya R, Das A, Prashar V, & Kumar M. Potential inhibitors against papain-like protease of novel coronavirus (SARS-CoV-2) from FDA approved drugs. *ChemRxiv*. doi: 26434/chemrxiv.1186001.v2 (2020).
20. Kumar Y, & Singh H. *In silico* identification and docking-based drug repurposing against the main protease of SARS-CoV-2, causative agent of COVID-19. *ChemRxiv* (2020).
21. Zhang H, Penninger J, Li Y, Zhong N, & Slutsky AS. Angiotensin-converting enzyme 2 (ACE2) as a SARS-CoV-2 receptor: molecular mechanisms and potential therapeutic target. *Intens Care Med* 46, 586–590. doi: 10.1007/s00134-020-05985-9 (2020c).
22. World Health Organization. Coronavirus disease (COVID-19): situation report-107. https://www.who.int>(2020).
23. Enayatkhani M, Hasaniazad M, Faezi S, Guklani H, Davoodian P, Ahmadi N, Ali Einakian M, Karmostaji A, Ahmadi K. Reverse vaccinology approach to design a novel multi-epitope vaccine candidate against COVID-19: an *in silico J. Biomol. Struct. Dyn*., 1-19. doi: 10.1080/07391102.2020.1756411(2020).

24. Boopathi S, Poma AB, & Kolandaivel P. Novel 2019 coronavirus structure, mechanism of action, antiviral drug promises and rule out against its treatment. *Biomol. Struct. Dyn.*, 1-14 (2020).
25. Kanchanapoom T, Kasai R, Chumsri P, Hiraga Y, & Yamasaki K. Canthin-6-one and β-carboline alkaloids from *Eurycoma harmandiana*. *Phytochemistry* 56, 383-386 (2001).
26. Ul Qamar MT, Maryam A, Muneer I, Xing F, Ashfaq UA, Khan FA, Anwar F, Geesi MH, Khalid RR, Rauf SA, & Siddiqi AR. Computational screening of medicinal plants phytochemicals to discover potent pan-seotype inhibitors against dengue virus. *Rep.* 9, 1433. https://doi.org/10.1038/s41598-018-38450-1 (2019).
27. Kim JH, Cho IS, So YK, Kim HH, & Y.H. Kim YH. Kushenol A and 8-prenylkaempferol, tyrosinase inhibitors, derived from *Sophora flavescens*. *Enzyme Inhib. Med. Chem*. 33, 1048-1054. doi:10.1080/14756366.2018.1477776 (2018).
28. Lin ZX, Che CT, Lee SS, Chan RCY, Ip PSP, & Yang JM. *Sophora flavescens* (Ku-Shen) as a booster for antiretroviral therapy through cytochrome P450 3A4 inhibition. *Health and Health Service Research Fund* 21, S18-21 (2015).
29. Mussard E, Cesaro A, Lespessailles E, Legrain B, Berteina-Raboin S, & Toumi H. Andrographolide, a natural antioxidant: an update. *Antioxidants* 8, 571. doi: 10.3390/qntiox8120571 (2019).
30. JayaKumar T, Hsieh CY, Lee JJ, & Sheu JR. Experimental and clinical pharmacology of Andrographis paniculate and its major bioactive phytoconstituent Andrographolide. *Based Complementary Altern. Med.*, 1-16. doi: 10.1155/2013/846740 (2013).
31. Rafi M, Devi AF, Syafitri UD, Heryanto R, Suparto IH, Amran MB, Rohman A, Prajogo B & Lim LW. Classification of *Andrographis paniculate* extracts by solvent extraction using HPLC fingerprint and chemometric analysis. *BMC Res Notes* 13, 56. https://doi.org/10.1186/s13104-020-4920-x (2020).
32. Churiyah POB, Rofaani E, & Tarwadi. Antiviral and immunostimulant activities of *Andrographis paniculate*. *HAYATI J Biosci* 22, 67-72. doi: 10.4308/hjb.22.2.67 (2015).
33. Wintachai P, Kaur P, Lee RCH, Ramphan S, Kuadkitkan A, Wikan N, Ubol S, Roytrakul S, Chu JJH, & Smith DR. Activity of andrographolide against chikungunya virus infection. *Rep*. 5, 14179. doi: 10.1038/srep14179 (2015).
34. Kim S, Thiessen PA, Bolton EE, Chen J, Fu G, Gindulyte A, Han L, He J, He S, Shoemaker BA, Wang J, Yu B, Zhang J, & Bryant SH. PubChem substance and compound databases. *Nucleic Acids Res*. 44, D1202–D1213 (2016).
35. Berman HM, Westbrook J, Feng Z, Gilliland G, Bhat TN, Weissig H, Shindyalov IN, & Bourne PE. The Protein Data Bank. *Nucleic Acids Res* 235-242 (2000).
36. The PyMOL Molecular Graphics System, Version 1.2r3pre, Schrödinger, LLC. https://pymol.org/2/(2020).
37. Dallakyan SO, & Arthur. Small-Molecule Library Screening by Docking with PyRx. *Methods Mol Biol* 1263, 243-250. 10.1007/978-1-4939-2269-7_19 (2015).
38. Trott O, & Olson AJ. AutoDock Vina: improving the speed and accuracy of docking with a new scoring function, efficient optimization, and multithreading. *Comput. Chem*. 31, 455-461. https://doi.org/10.1002/jcc.21334 (2010).
39. Dassault Systèmes BIOVIA, Discovery Studio, Release 2020, San Diego: Dassault Systèmes, (2020).
40. Lu H, Stratton CW, & Tang YW. Outbreak of Pneumonia of Unknown Etiology in Wuhan China: the Mystery and the Miracle. *Med. Virol*. 92, 401-402. doi: 10.1002/jmv.25678 (2020).
41. Chen Y, Liu Q, & Guo D. Emerging coronaviruses: genome structure, replication, and pathogenesis. *Med. Virol*. 92, 418-423 (2020).
42. Malik YS, Sircar S, Bhat S, Sharun K, Dhama K, Dadar M, et al, Emerging novel coronavirus (2019-nCoV)—current scenario, evolutionary perspective based on genome analysis and recent developments. *Vet Q*40, 68-76 (2020).
43. Andersen KG, Rambaut A, Lipkin WI, Holmes EC, & Garry RF. The proximal origin of SARS-CoV-2. *Med.*26, 450-452 (2020).
44. Shah B, Modi P, & Sagar SR. *In silico* studies on therapeutics agents for COVID-19: drug repurposing approach. *Life Sci* 252, 117652. doi: 10.1016/j.lfs.2020.117652 (2020).
45. Pinzi L, & Rastelli G. Molecular docking: shifting paradigms in drug discovery. *J. Mol. Sci.* 20, 4331. doi: 10.3390/ijms20184331 (2019).
46. Prajapat M, Sarma P, Shekhar N, Avti P, Sinha S, Kaur H, Kumar S, Bhattacharyya A, Kumar H, Bansal S, & Medhi B. Drug target for corona virus: a systematic review. *Indian J. Pharmacol* 52, 56-65. doi: 10.4103/ijp.IJP_115_20 (2020).
47. Gautret P, Lagier JC, Parola P, Meddeb L, Mailhe M, Doudier B, et al. Hydroxychloroquine and azithromycin as a treatment of COVID-19: results of an open-label non-randomized clinical trial. *J. Antimicrob. Agents*, 105949 (2020).
48. Mitjà O, & Clotet B. Use of antiviral drugs to reduce COVID-19 transmission. *Lancet Glob Health*8, e639-e640 (2020).
49. Wu R, Wang L, Dina Kuo HC, Shannar A, Peter R, Chou PJ, Li S, Hudlikar R, Liu X, Liu Z, Poiani GJ, Amorosa L, Brunetti L, & Kong AN. An update on current therapeutic drugs treating COVID-19. *Pharmacol. Rep*. 11, 1-15. doi: 10.1007/s40495-020-00216-7 (2020).
50. Elfiky AA. Ribavirin, Remdesivir, Sofosbuvir, Galidesivir, and Tenofovir against SARS-CoV-2 RNA dependent RNA polymerase (RdRp): A molecular docking study. *Life sci.*, 117592 (2020).
51. Barratt E, Bingham RJ, Warner DJ, Laughton CA, Phillips SE, & Homans SW. Van der Waals interactions dominate ligand− protein association in a protein binding site occluded from solvent water. *Am. Chem. Soc.*127, 11827-11834 (2005).
52. Meng XY, Zhang HX, Mezei M, Cui M. Molecular docking: a powerful approach for structure-based drug discovery. *Curr Comput-Aid Drug* 7, 146-157 (2011).

53. Daina A, Michielin O, & Zoete V. SwissADME: a free web tool to evaluate pharmacokinetics, drug-likeness and medicinal chemistry friendliness of small molecules. *Rep*. 7, 42717 (2017).
54. Han Y, Zhang X, Zhang J, & Hu CQ. *In silico* ADME and toxicity prediction of ceftazidime and its impurities. *Pharmacol.* 10, 434 (2019).
55. Daneman R, & Prat A. The blood–brain barrier, Cold Spring Harb. *Biol*. 7, a020412 (2015).
56. Pajouhesh H, & Lenz GR. Medicinal chemical properties of successful central nervous system drugs. *NeuroRx* 2, 541-553 (2005).
57. Chen CP, Chen CC, Huang CW, & Chang YC. Evaluating molecular properties involved in transport of small molecules in stratum corneum: a quantitative structure-activity relationship for skin permeability. *Molecules* 23, 911 (2018).
58. Das S, Sarmah S, Lyndem S, & Roy AS. An investigation into the identification of potential inhibitors of SARS-CoV-2 main protease using molecular docking study. *Biomol. Struct. Dyn*. doi: 10.1080/07391102.2020.1763201 (2020).
59. Salim B, & Noureddine M. Identification of compounds from Nigella sativa as new potential inhibitors of 2019 novel coronaviruses (covid-19): molecular docking study. *ChemRxiv*. doi: 20944/preprints202004.0079.v1 (2020).
60. McKee DL, Sternberg A, Stange U, Laufer S, & Naujokat C. Candidate drugs against SARS-CoV-2 and COVID-19. *Pharmacol Res* 157, 104859. https://doi.org/10.1016.phrs.2020.104859 (2020).
61. Aanouz I, Belhassan A, El-Khatabi K, Lakhlifi T, El-Idrissi M, & Bouachrine M. Moroccan medicinal plants as inhibitors against SARS-CoV-2 main protease: computational investigation. *J Biomol Struct Dyn*. doi: 10.1080/07391102.2020.1758790 (2020).
62. Kumar D, Kumari K, Jayaraj A, Kumar V, Kumar RV, Dass SK, Chandra R, & Singh P. Understanding the binding affinity of noscapines with protease of SARS-CoV-2 for COVID-19 using MD simulations at different temperatures. *Biomol. Struct. Dyn.*, 1-14. DOI: 10.1080/07391102.2020.1752310 (2020a).
63. Kumar V, Dhanjal JK, Kaul SC, Wadhwa R, & Sundar D. Withanone and Caffeic Acid Phenethyl Ester are Predicted to Interact with Main Protease (Mpro) of SARS-CoV-2 and Inhibit its Activity. *Biomol. Struct. Dyn.*, 1-17 (2020b).
64. Lobo-Galo N, Terrazas-López M, Martínez-Martínez A, & Díaz-Sánchez AG. FDA-approved thiol-reacting drugs that potentially bind into the SARS-CoV-2 main protease, essential for viral replication. *Biomol. Struct. Dyn.*,1-12 (2020).
65. Sharma A, Tiwari S, Deb MK, & Marty JL. Severe acute respiratory syndrome coronavirus-2 (SARS-CoV-2): a global pandemic and treatment strategies. *J. Antimicrob. Agents* 10, 106054. doi: 10.1016/j.ijantimicagh.2020.106054 (2020).
66. Tallei T, Tumilaar SG, Niode N, Fatimawali F, Kepel B, Idroes R, & Effendi Y. Potential of plant bioactive compounds as SARS-CoV-2 main protease (Mpro) and spike (S) glycoprotein inhibitors: a molecular docking study. doi: 10.20944/preprints202004.0102.v2 (2020).
67. Subhomoi B, & Banerjee M. A computational prediction of SARS-CoV-2 structural protein inhibitors from *Azadirachta indica* (Neem). *Biomol. Struct. Dyn.* Doi: 10.1080/07391102.2020.1774419 (2020).
68. Arthur DE, & Uzairu A. Molecular docking studies on the interaction of NCI anticancer analogues with human Phosphatidylinositol 4, 5-bisphosphate 3-kinase catalytic subunit. *King Saud Univ. Sci.* 31, 1151-1166 (2019).
69. Enmozhi SK, Raja K, Sebastine I & Joseph J. Andrographolide as a potential inhibitor of SARS-CoV-2 main protease: an *in-silico J. Biomol. Struct. Dyn.* https://doi.org/10.1080/07391102.2020.1760136 (2020).

Note For Tables

Due to technical limitations, full-text HTML conversion of Table 2 could not be completed. However, the table can be downloaded and accessed as a PDF in the supplementary files.

Figures

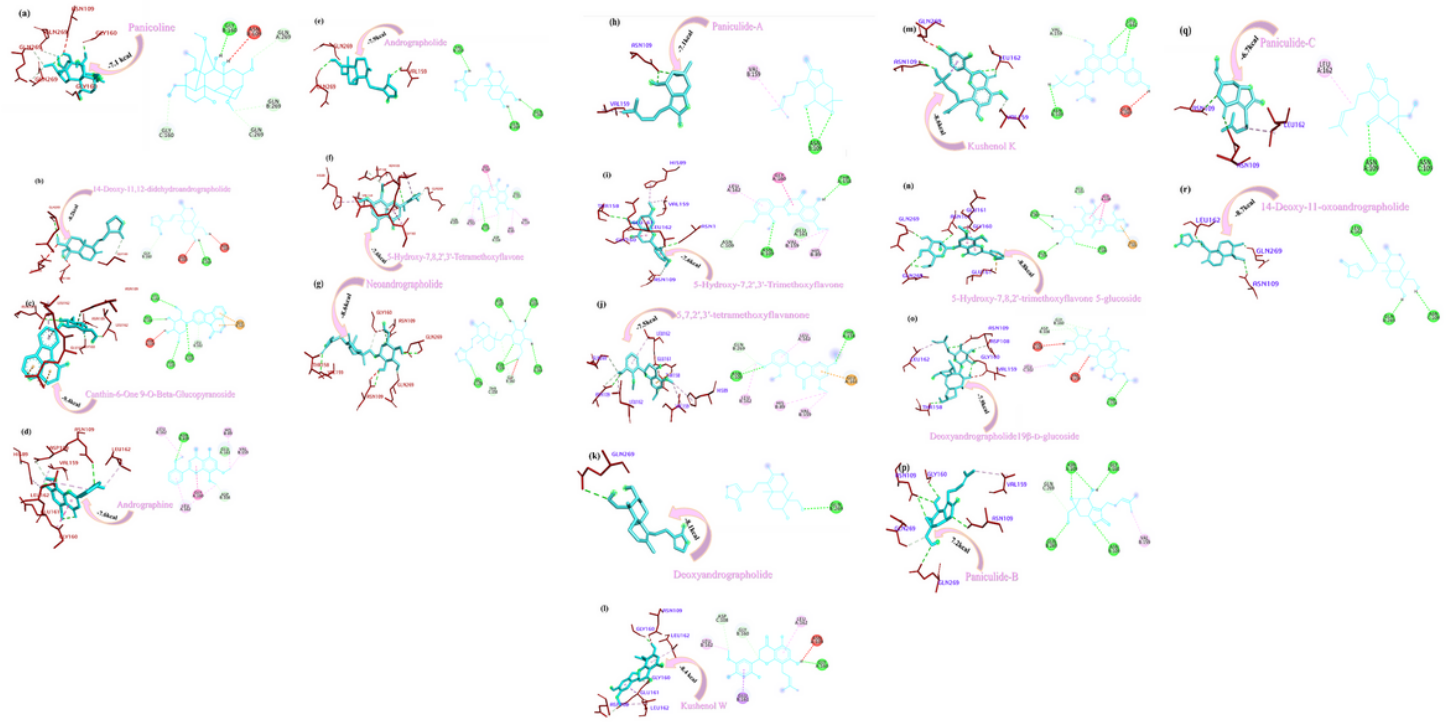

Figure 1

Interactions established after docking the secondary metabolite against SARS CoV-2 PLpro Protein (6W9C).The interacting residues of protein are labelled in purple and the docking scores are listed under each of the complex, respectively. The receptor-ligand interaction is represented on a 3D diagram (Right) and 2D diagram (Left). Drugs are in cyan and interacting atoms of protein is represented red in the diagram, while green dotted lines represents the conventional h-bond interactions, light green dotted lined represents weak vander wall interactions. Additionally, dotted lines in sky blue displays the pi-donar hydrogen bond, pi-sigma interaction is shown as violet dashed lines, baby pink dotted lines shows alkyl and pi-alkyl interactions respectively.

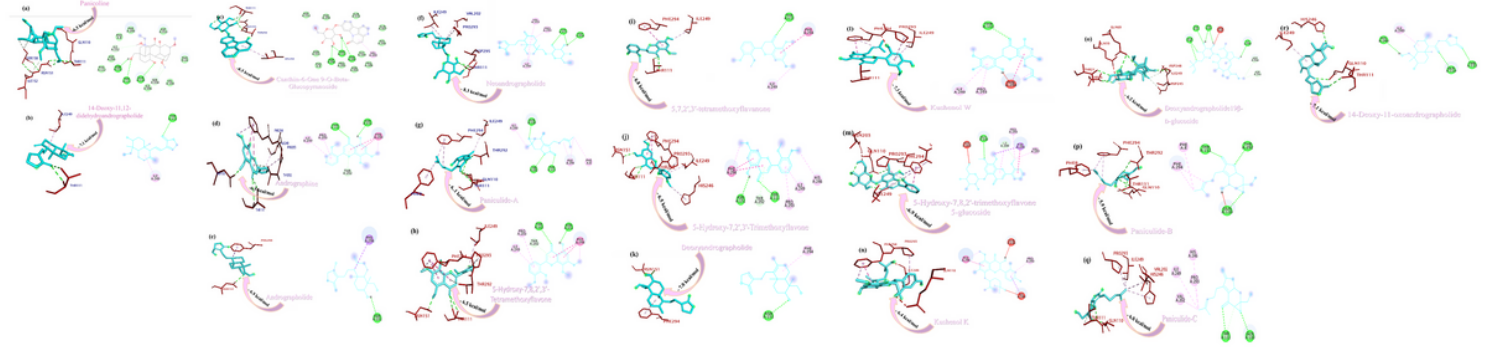

Figure 2

Interactions established after docking the secondary metabolite against SARS CoV-2 Mpro/3CLpro Protein (6M2N). The interacting residues of protein are labelled in purple and the docking scores are listed under each of the complex, respectively. The receptor-ligand interaction is represented on a 3D diagram (Right) and 2D diagram (Left). Drugs are in cyan and interacting atoms of protein is represented red in the diagram, while green dotted lines represents the conventional h-bond interactions, light green dotted lined represents weak vander wall interactions. additionally, dotted lines in sky blue displays the pi-donar hydrogen bond, pi-sigma interaction is shown as violet dashed lines, baby pink dotted lines shows alkyl and pi-alkyl interactions respectively.

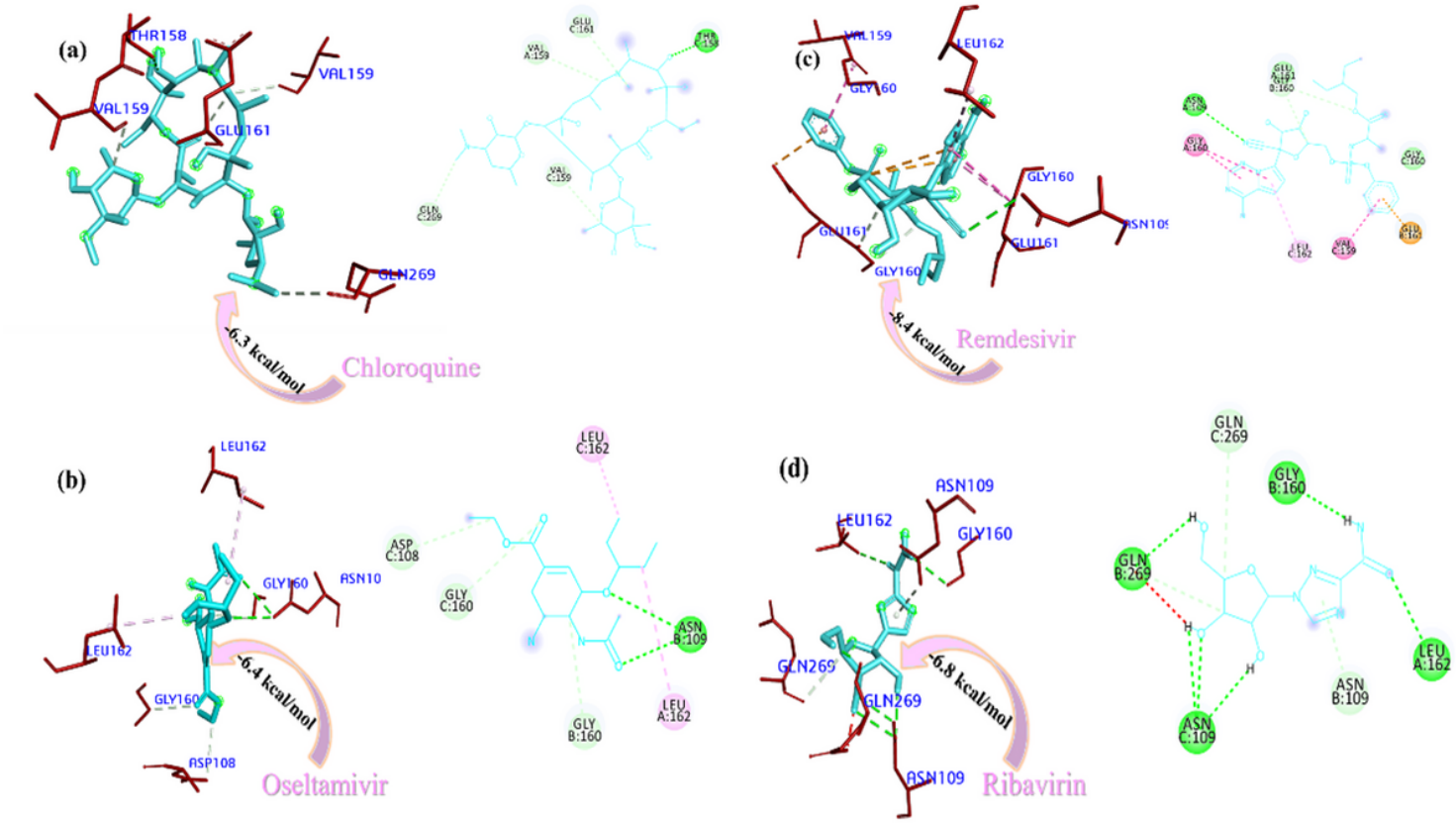

Figure 3

Interactions established after docking the drugs against SARS CoV-2 PLpro Protein (6W9C). The receptor-ligand interaction is represented on a 3D diagram (Right) and 2D diagram (Left). The interacting residues of protein are labelled in purple and the docking scores are listed under each of the complex, respectively. Drugs are in cyan and interacting atoms of protein is represented red in the diagram, while green dotted lines represents the conventional h-bond interactions, light green dotted lined represents weak vander wall interactions. additionally, dotted lines in sky blue displays the pi-donar hydrogen bond, pi-sigma interaction is shown as violet dashed lines, baby pink dotted lines shows alkyl and pi-alkyl interactions respectively.

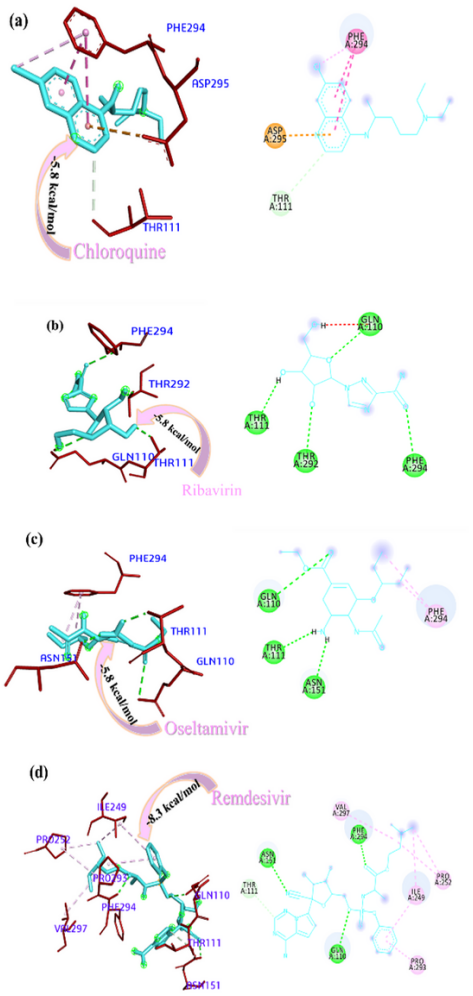

Figure 4

Interactions established after docking the drugs against SARS CoV-2 Mpro/3CLpro Protein (6M2N). The interacting residues of protein are labelled in Purple and the docking scores are listed under each of the complex, respectively. The receptor-ligand interaction is represented on a 3D diagram (right) and 2D diagram (left). Drugs are in cyan and interacting atoms of protein is represented red in the diagram, while green dotted lines represents the conventional h-bond interactions, light green dotted lined represents weak vander wall interactions. additionally, dotted lines in sky blue displays the pi-donar hydrogen bond, pi-sigma interaction is shown as violet dashed lines, baby pink dotted lines shows alkyl and pi-alkyl interactions respectively.

Supplementary Files

This is a list of supplementary files associated with this preprint. Click to download.

- Table2.pdf